Applied Physics Letters

Voltage control of magnetism with magneto-ionic approaches: Beyond voltage-driven oxygen ion migration

Cite as: Appl. Phys. Lett. **120**, 070501 (2022); https://doi.org/10.1063/5.0079762
Submitted: 24 November 2021 • Accepted: 01 February 2022 • Published Online: 16 February 2022

J. de Rojas, A. Quintana, G. Rius, et al.

COLLECTIONS

This paper was selected as Featured

View Online Export Citation CrossMark

ARTICLES YOU MAY BE INTERESTED IN

Random alloy thick AlGaAsSb avalanche photodiodes on InP substrates
Applied Physics Letters **120**, 071101 (2022); https://doi.org/10.1063/5.0067408

Advances in magneto-ionic materials and perspectives for their application
APL Materials **9**, 030903 (2021); https://doi.org/10.1063/5.0042544

Spectral modulation of blocked-impurity-band hybrid structure terahertz detector
Applied Physics Letters **120**, 071102 (2022); https://doi.org/10.1063/5.0082048

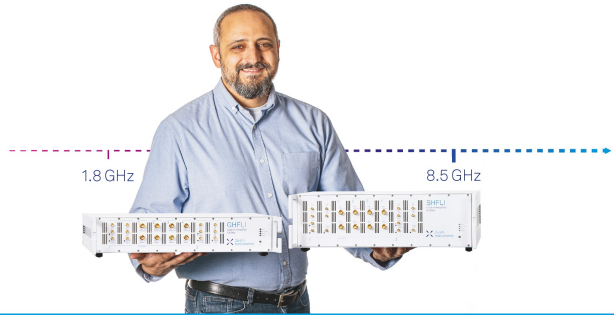

Trailblazers. New
Meet the Lock-in Amplifiers that measure microwaves.
Zurich Instruments
Find out more

© 2022 Author(s).

Applied Physics Letters PERSPECTIVE scitation.org/journal/apl

Voltage control of magnetism with magneto-ionic approaches: Beyond voltage-driven oxygen ion migration

Cite as: Appl. Phys. Lett. **120**, 070501 (2022); doi: 10.1063/5.0079762
Submitted: 24 November 2021 · Accepted: 1 February 2022 ·
Published Online: 16 February 2022

View Online Export Citation CrossMark

J. de Rojas,[1,a] A. Quintana,[2] G. Rius,[3] C. Stefani,[4] N. Domingo,[4] J. L. Costa-Krämer,[5] E. Menéndez,[1,a] and J. Sort[1,6,a]

AFFILIATIONS

[1]Departament de Física, Universitat Autònoma de Barcelona, Cerdanyola del Vallès E-08193, Spain
[2]Institut de Ciència de Materials de Barcelona (ICMAB-CSIC), Campus UAB, Cerdanyola del Vallès E-08193, Spain
[3]Institut de Microelectrònica de Barcelona (IMB-CNM-CSIC), Campus UAB, Cerdanyola del Vallès E-08193, Spain
[4]Catalan Institute of Nanoscience and Nanotechnology (ICN2), CSIC and BIST, Campus UAB, Cerdanyola del Vallès E-08193, Spain
[5]IMN-Instituto de Micro y Nanotecnología (CNM-CSIC), Isaac Newton 8, PTM, Tres Cantos, Madrid E-28760, Spain
[6]Institució Catalana de Recerca i Estudis Avançats (ICREA), Pg. Lluís Companys 23, Barcelona E-08010, Spain

[a]**Authors to whom correspondence should be addressed:** juliuscaesar.derojas@uab.cat; enric.menendez@uab.cat; and jordi.sort@uab.cat

ABSTRACT

Magneto-ionics is an emerging field in materials science where voltage is used as an energy-efficient means to tune magnetic properties, such as magnetization, coercive field, or exchange bias, by voltage-driven ion transport. We first discuss the emergence of magneto-ionics in the last decade, its core aspects, and key avenues of research. We also highlight recent progress in materials and approaches made during the past few years. We then focus on the "structural-ion" approach as developed in our research group in which the mobile ions are already present in the target material and discuss its potential advantages and challenges. Particular emphasis is given to the energetic and structural benefits of using nitrogen as the mobile ion, as well as on the unique manner in which ionic motion occurs in CoN and FeN systems. Extensions into patterned systems and textures to generate imprinted magnetic structures are also presented. Finally, we comment on the prospects and future directions of magneto-ionics and its potential for practical realizations in emerging fields, such as neuromorphic computing, magnetic random-access memory, or micro- and nano-electromechanical systems.

© 2022 Author(s). All article content, except where otherwise noted, is licensed under a Creative Commons Attribution (CC BY) license (http://creativecommons.org/licenses/by/4.0/). https://doi.org/10.1063/5.0079762

The proliferation of modern electronic devices continues at a furious pace, integrated into everything from advanced scientific equipment to everyday household items. They form the backbone of technologies, such as the Internet of Things, Artificial Intelligence, and Big Data—technologies pushing current computer hardware and architectures to their limits, both in terms of functionality and energy efficiency. Functionally, the ubiquitous von Neumann architecture found in nearly all computers, while excellent at computing many sequential tasks very quickly, struggles to perform complex tasks, such as pattern recognition on large but imprecise or incomplete data sets. The biological brain, however, performs such task orders of magnitude more efficiently, inspiring neuromorphic computing,[1] a paradigm, which mimics the structure of the biological brain by de-centralizing duties away from single-task units and redistributing both memory and computation functions among a large number of neurons connected by synapses. Realizing such structures requires moving beyond volatile hardware units and relying instead on hardware able to offer analog tuning of properties depending on the stimulus provided, allowing for "learning" and "forgetting" functionalities, among others. In terms of energy efficiency, concerns regarding production and development portend the death of conventional hardware in the coming 10–15 years. Neural networks have applied neuromorphic principles to conventional computer hardware with tremendous effect,[2–4] but fundamental issues, such as manufacturing limitations, the

© Author(s) 2022

so-called dark or dim silicon, and power and cooling restraints have already left current devices struggling to maintain efficiency at dimensions $\lesssim$10 nm,[5,6] sparking a search for life after Moore's Law.[7] Spintronics[8,9] has enjoyed success using spin-polarized current to induce low-power magnetization reversal via spin-transfer torque[10,11] or spin–orbit torque,[12,13] but these still rely heavily on electric current to manipulate magnetic elements, leading to Joule heating. This concern also extends to, among other technologies, micro- and nanoelectromechanical systems (MEMS and NEMS) and hard disk drives, where current is used to manipulate magnetic elements. These challenges, coupled with expected worldwide electricity demands and environmental impacts of existing technology,[14–16] have led to an intense search for low-power, energy-efficient materials with flexible functionalities. One proposed solution to this challenge is the use of an applied external electric field, instead of current, to modulate the magnetic properties of a material. The expanding number of materials and mechanisms that produce this effect has grown into a field of research broadly classified as voltage control of magnetism (VCM).[17–22]

The intrinsic coupling between an applied magnetic (electric) field and a medium's electric polarization (magnetization) was first proposed by P. Curie when discussing the Wiedemann effect,[23] a coupling later coined the *magnetoelectric effect* (ME) by Debye.[24] Landau and Lifshitz postulated a linear ME effect in select magnetic crystal symmetry classes,[25] which Dzyaloshinskii extended to predict its existence in Cr_2O_3,[26] confirmed by experiment soon after.[27–30] This sets the stage for the pursuit of ME effects in single-phase multiferroics,[31,32] a class of material, which exhibits two or more types of ferroic order.[33] However, the fundamental requirements for a material to possess both ferroelectric and ferromagnetic order make multiferroics rare,[34] pushing research beyond single-phase materials. Composite materials[35–40] generate the ME effect by stitching together two ferroic phases, coupled by some mediating mechanism. Piezo-strain mediated ME effects utilize lattice changes in a ferroelectric material under bias to "strain" a magnetic material, inducing a change in its magnetic properties.[41–50] Carrier density-mediated ME effects rely on an applied electric field to tune surface charge density in magnetic semiconductors,[51–54] ultrathin metallic films,[55–59] and complex magnetic oxides sensitive to carrier doping at the interface of complex-oxide heterostructures.[60–64] Exchange bias-mediated ME effects, where the interfacial exchange interaction between an antiferromagnetic ferroelectric and a ferromagnetic layer results in a biasing of the magnetization curve away from zero, can be controlled by applying voltage to the ferroelectric layer in several systems.[65–70] Orbital reconstruction ME effects[71] occur when an applied field induces orbital reconstructions and hybridizations of atoms at the boundary between layers.[72–77] To these, we add a rapidly growing sub-field of VCM, the electrochemical effect, which has only emerged within the last decade. Dielectrics, such as ionic liquids, GdO_x, HfO_2, AlO_x, Y_2O_3-doped ZrO_2, and $SrCoO_{2.5}$,[78–86] have opened up the possibility to significantly alter the oxidation states of an adjacent material. The electrochemical effect is generally split into two mechanisms: electrostatic (charging) effects and magneto-ionics. The presence of both effects was shown in ultra-thin $La_{0.5}Sr_{0.5}MnO_{3-\delta}$,[87] with negative bias, inducing reversible hole accumulation (electrostatic), and positive bias, inducing irreversible oxygen vacancy formation (magneto-ionics). Strictly electrostatic effects were demonstrated in the magnetic oxide semiconductor $(Co,Ti)O_2$,[88] while Walter *et al.*[89] very recently demonstrated the fascinating result that diamagnetic (zero-spin) FeS_2 could be biased into a ferromagnetic state by electrostatically induced band filling alone. The evolution of VCM and some important milestones are presented in the top timeline of Fig. 1(a), with selected works referenced.

Magneto-ionics[83,84] first appeared in ultra-thin Co films adjacent to GdO_x, accomplished by inducing redox reactions at the interface under an applied bias, changing its magnetic state. A representative schematic of a typical magneto-ionic structure is shown in Fig. 1(b): a dielectric (either liquid or solid-state) is placed in contact with a target material (which maybe an oxide or a metal), with voltage applied across the film and dielectric, inducing ionic motion. More generally, magneto-ionics uses an applied electric field to insert ions into and remove them from a target material, undergoing changes in

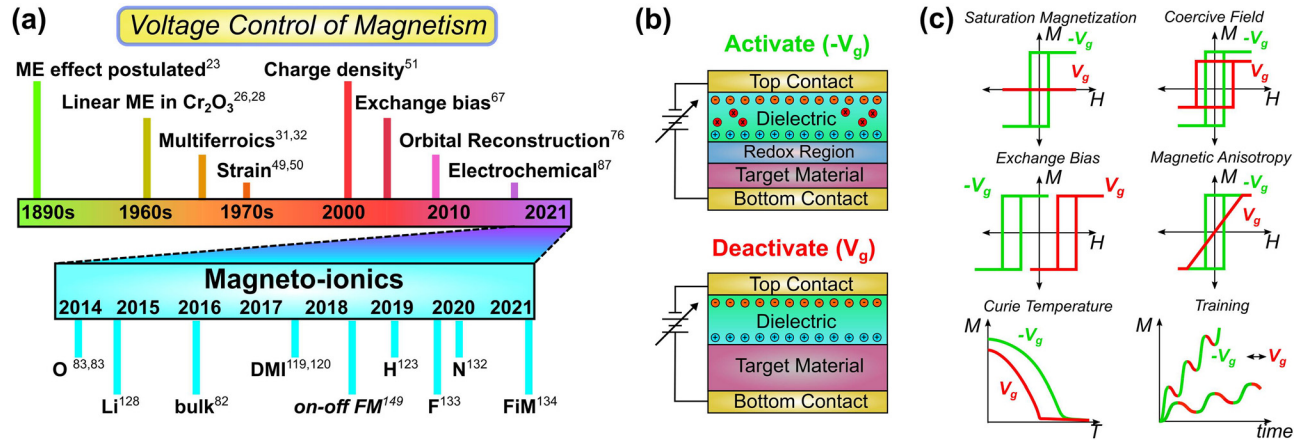

FIG. 1. (a) Timeline noting representative milestones in voltage control of magnetism and recent developments in magneto-ionics. (b) Schematic of a generic magneto-ionic device common to many systems, with the gate voltage V_g setting or resetting a magnetic state via a redox reaction. Dielectric may be a liquid or solid-state electrolyte, and the activated region may correspond to the interface or beyond the interface into the bulk. Large red circles indicate the ions, which flow toward or away from the target material under bias, such as O^{2-}, H^+, Li^+, N^{3-}, or F^-. (c) Sketch of some magnetic parameters which may be turned in a magneto-ionic system, including saturation magnetization, coercive field, exchange bias, magnetic anisotropy, and Curie Temperature.[82,90–97]

© Author(s) 2022

stoichiometry, oxidation state, crystalline structure, as well as large and cyclable changes in magnetic properties [Fig. 1(c)].[82,90–97] Magneto-ionic materials also offer several potential advantages for practical applications: They potentially require lower energy to actuate (as low ≈10 aJ/bit,[98,99] much lower than traditional current-using methods, ≈10 fJ/bit[100]), no voltage to maintain a set state (nonvolatile) and offer the possibility of functional plasticity (i.e., the ability to undergo non-volatile changes in its structure and properties in response to an external stimulus), making magneto-ionic materials intriguing candidates to be deployed in neuromorphic or stochastic computing, magnetic random access memory, domain-wall logic, and lab-on-a-chip devices.[101–103] Indeed, magneto-ionics has already been identified for potential use in several applications. Magnetic actuation is key in microelectromechanical systems,[104–107] where magneto-ionics may prove utile in fabricating multifunctional robotic materials.[108] The use of ionic transport to modify magnetic properties has already been observed in Pt/Co(Fe)/MgO, Ta/CoFeB/MgO, and Pt/Co/Ni/HfO_2 stacks,[79,109,110] representative structures for magnetic random-access memories[58,111] and envisioned to allow for low-power tunability of the switching elements via the insulating tunnel barrier. Spin textures, such as skyrmions,[112,113] chiral domain walls,[114,115] and spin spirals,[116,117] are stabilized under the Dzyaloshinskii–Moriya interaction (DMI), which have been shown to be tunable using magneto-ionics,[118–121] with possible applications in spin-orbitronics.[122] Continued fundamental research has led to further exploration of different structures, materials, and mobile ions, with successful demonstration of magneto-ionic effects using hydrogen,[118,123–125] lithium,[126–130] nitrogen,[131–133] and flourine.[134] The last two years have seen a flurry of exciting activity, a few of which are highlighted in Fig. 2. In 2019, Tan *et al.*[123,124] showed that insertion of H^+ into the interface of Co/GdO_x stacks increased the speed of nondestructive toggling of magnetic anisotropy, demonstrating that the powerful contribution of H^+ plays in altering Co oxidation state under voltage, while recent work by Huang *et al.* has shown voltage-control of the sublattice in ferrimagnetic GdCo and toggling magnetic order.[135] Yi *et al.*[91] reported reversible and nonvolatile phase transitions at room temperature under voltage using both H^+ and O^{2-} ions in digital complex oxides, showing that nondestructive structural changes under bias are possible [Fig. 2(a)]. Murray *et al.*[136] demonstrated that exchange bias can be controlled in Gd/$Ni_{1-x}Co_xO$ thin films [Fig. 2(b)], where interfacial $Ni_{1-x}Co_xO$ is reduced to magnetic NiCo to establish an exchange bias that can be modulated by up to 35% under voltage conditioning. Zehner *et al.* and Mustafa *et al.* also showed the ability to tune exchange bias under voltage by inducing redox reactions due to O^{2-} and Li^+, respectively.[125,137,138] Chen *et al.*[118] reported inducing Dzyaloshinskii-Moriya interaction by chemisorption and desorption of H^+, seen in reversible and nonvolatile chirality transitions of magnetic domain walls [Fig. 2(c)]. Navarro-Senet *et al.*[139,140] and Robbennolt *et al.*[141,142] have produced dramatic electric field induced changes in the magnetic properties of nanoporous, mesoporous, and nanostructured materials with high surface-to-volume ratios, extending magneto-ionic phenomena beyond thin film structures [Fig. 2(d)].

The changes occurring primarily by redox reactions at the interface of heterostructures have motivated studies of magneto-ionic effects in thin metal films. However, systems that utilize target ferromagnetic metal layers, such as Co, are limited to ultra-thin films (≲5 nm), where patterning on the nanoscale leaves them susceptible

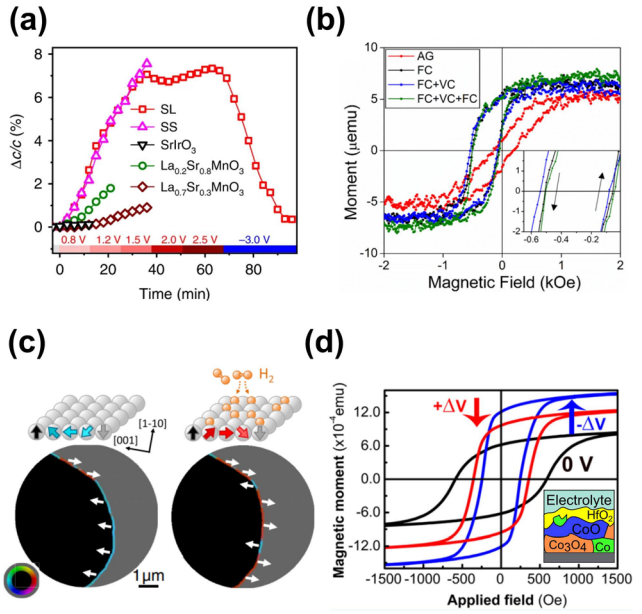

FIG. 2. Examples of recent progress in magneto-ionics. (a) Modulation of out-of-plane lattice constant (Δc/c) during voltage cycling [SS refers to $Sr(Mn_{0.5}Ir_{0.5})O_3$ and SL refers to $[(La_{0.2}Sr_{0.8}MnO_3)_1(SrIrO_3)_1]_{20}$], showing reversible structural changes in the digital oxide (SL). Adapted with permission from Yi *et al.*, Nat. Commun. **11**, 902 (2020). Copyright 2020 Springer Nature. (b) Hysteresis loops of a Gd/$Ni_{0.5}Co_{0.5}O$ sample in the as-grown state, after field cooling, subsequent voltage conditioning, and followed by a second field cooling, showing enhanced exchange bias. Adapted with permission from Murray *et al.*, ACS Appl. Mater. Interfaces **13**(32) 38916–38922 (2021). Copyright 2021 American Chemical Society. (c) Observation of hydrogen-induced domain-wall chirality switching in compound spin polarized low energy electron microscopy (SPLEEM), showing as-grown (left) and hydrogen exposed (right) states. Black and gray areas indicate perpendicularly magnetized up and down domains, and colors indicate the in-plane orientation of magnetization in the domain-wall region. Adapted with permission from Chen *et al.*, Phys. Rev. X **11**, 021015 (2021). Copyright 2021 American Physical Society. (d) Room-temperature in-plane VSM measurements of nanostructured metallic alloys conformally coated with insulating oxide nanolayers (Co−Pt/HfO_x) under −50 and +100V, applied for 90 min. Adapted with permission from Navarro-Senent *et al.*, ACS Appl. Mater. Interfaces **12**, 14484–14494 (2020). Copyright 2020 American Chemical Society.

to superparamagnetic transitions and often lack nonvolatile states. In addition, oxygen ion migration has often required heat assistance to aide ion mobility,[82,84,123,124,143] reducing potential energy efficiency. Effects beyond the interface have also been explored, although this brings the added complication of relatively large oxygen ions moving through the film, resulting in irreversible structural or compositional changes as the ions move along grain boundaries and fill vacancies, limiting reversible toggling to redox reactions at the interface.[82,119,144,145] As a simple illustration, consider that in the transition from metallic Co to CoO, the change in relative cobalt positions while changing phase would approach 20%. To improve cyclability and durability, these kinds of stresses and distortions should be minimized, potentially by using the migrating ion in the as-deposited state. Oxide/metal heterostructures in thin films and islands have been explored using Fe/FeO_x[96,146] and Co/CoO_x structures, allowing the reversible removal and insertion of oxygen to toggle magnetic states. In

© Author(s) 2022

particular, *on-off* switching of magnetism has been observed in iron-based hybrid transition metal oxide/metal,[90,140,147] transition metal oxide[148–151] films, and porous structures. Along this vein, we discuss our recent work on the structural-ion approach, where the target material possesses the migrating anions in the as-deposited state, in single layer oxide and nitride films, and so providing a crystal structure with more local vacancies and larger ionic pathways, facilitating ion movement in and out of the target material with reduced structural distortion.

We begin with magneto-ionics using the structural oxide approach in spinel Co_3O_4 films.[150,152] 100 nm-thick Co_3O_4 films, prepared by plasma-enhanced atomic layer deposition onto SiO_2, were voltage biased using propylene carbonate (PC) with solvated Na^+ ions. PC is a polar anhydrous liquid electrolyte, which generates a very large electric field with low voltage due to an electric double layer (EDL), allowing for magneto-ionic effects. Representative hysteresis loops of magnetization, *M*, as a function of applied magnetic field, *H*, measured by vibrating sample magnetometry (VSM) before and after the application of voltage, are shown in Fig. 3(a). The as-grown Co_3O_4 film initially shows no ferromagnetic signal, but after biasing under −10 V for 60 min, it shows an apparent hysteresis loop, clear evidence of a ferromagnetic response (*on*). This ferromagnetic signal is completely removed by subsequently applying a bias of +20 V for 60 min (*off*), i.e., demonstrating nonvolatile *on-off* control of ferromagnetism at room temperature. Additionally, the magneto-ionic response is found to scale with the increasing voltage; a series of biases (−10, −25, and −50 V) applied for 60 min results in increasing saturation magnetization, M_S, a result of increased voltage-driven ion migration and further reduction of Co_3O_4 to a metallic Co phase. The series was performed on the same film after applying a positive bias to return the sample to its original magnetic state (*off*), showing that cyclability is possible on the scale of 10^2 s, achievable without thermal assistance. *On* states are observed to have excellent stability, remaining steady and nonvolatile for months after *on-off* toggling. (Before and after *M–H* loops are provided in the supplementary material.) Interestingly, the redox process is found to penetrate deep into the film and, under high applied voltage (−200 V), introduces strong compositional and structural inhomogeneities, as observed by high-angle annular dark-field scanning transmission electron microscopy (HDAAF-STEM) and electron energy loss spectroscopy (EELS).[150] In the top figures of Fig. 3(b), it is clear that the Co and O distributions are isotropic across the film, consistent with Co_3O_4. In the bottom figures of Fig. 3(b), biasing at −200 V clearly reveals a mixture of Co and O concentrations. The ion flow is funneled through irregular O-rich diffusion

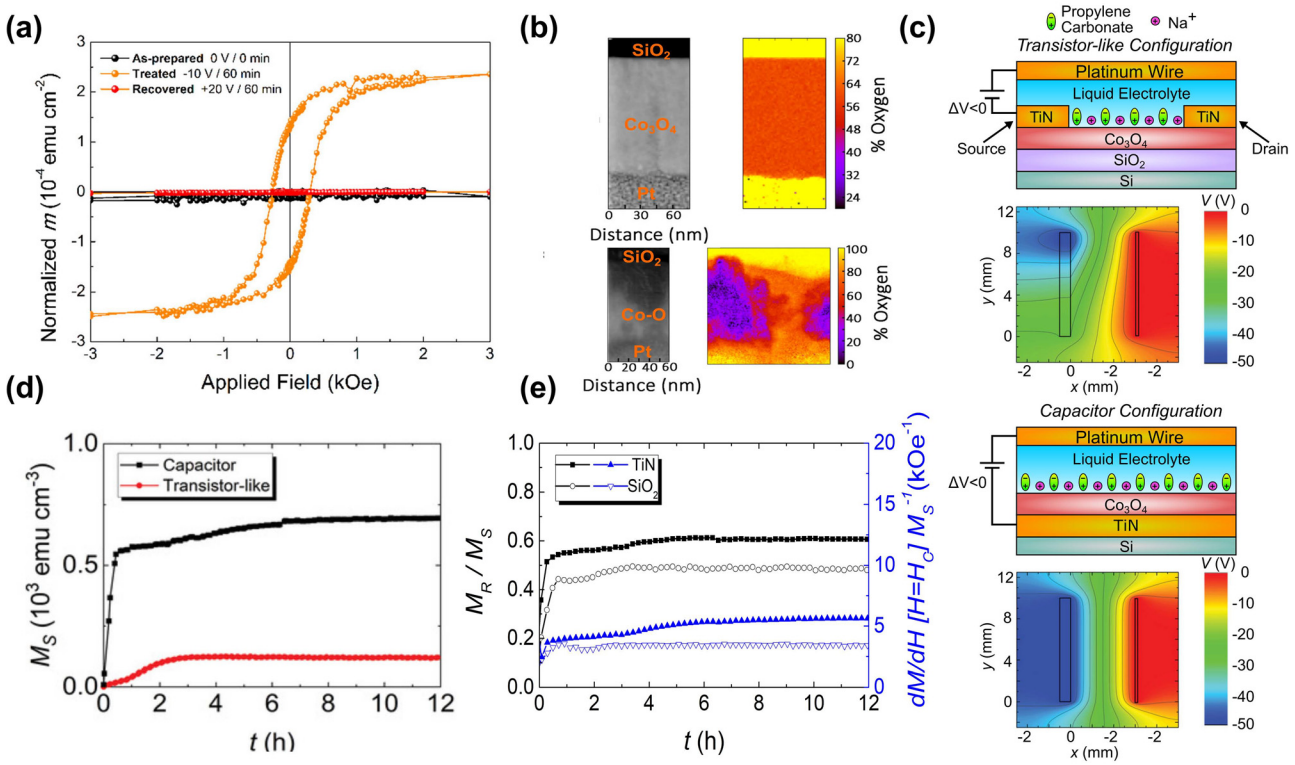

FIG. 3. (a) Normalized magnetic moment, *m*, vs applied magnetic field, *H*, of the as-grown Co_3O_4, the sample treated at −10 V for 60 min, and subsequently treated at +20 V for 60 min. (b) HAADF, Co and O EELS mappings of a sample negatively biased at –200 V for 30 min, respectively. Adapted with permission from Quintana *et al.*, ACS Nano **12**(10), 10291–10300 (2018). Copyright 2021. American Chemical Society. (c) COMSOL simulations of the initial voltage distribution at the moment the transistor-like (top) and the capacitor-like (bottom) configurations are biased. (d) Time evolution of the saturation magnetization (M_S vs *t*) and (e) squareness (M_R/M_S) and slope of hysteresis loop at the coercive field, H_C, normalized to M_S for the capacitor- and transistor-like configurations. Adapted with permission from de Rojas *et al.*, Adv. Funct. Mater. **30**, 2003704 (2010). Copyright 2020 John Wiley and Sons.

© Author(s) 2022

channels, which are highly nanostructured or partially amorphous, leaving Co-rich areas in its wake. Fascinatingly, the Co-rich and O-rich regions are formed by a combination of redistribution of cobalt and oxygen within the film, as well as oxygen moving toward the liquid electrolyte. Structural-ion systems also possess nonvolatile properties, which can be applied to neuromorphic architectures, where tuning of oxidation states as a function of depth in the film leads to continuous, analog changes in M_S, coercive field, H_c, or the switching field distribution (SFD), allowing for hysteretic "learning" or "forgetting" processes depending on the strength and duration of the applied field. To further extend the utility of cobalt oxide, the effects of the gating configuration on magneto-ionic speed were investigated by comparing transistor-like with capacitor-like configurations on two identically sputtered Co_3O_4 films. To understand the effects of device configuration, numerical simulations, modeling the initial voltage distributions for each configuration upon electrolyte-gating, were performed. The results show a stark difference in the electric potential of each configuration [see Fig. 3(c)]. The transistor-like configuration, due to the limited conductivity of Co_3O_4 and the insulating nature of the SiO_2 buffer layer, results in an inhomogeneous electric field along the film's length and width, weakening further away from the electrical TiN contact. The capacitor configuration, on the other hand, forms a nearly uniform electric field distribution along the length/width of the film (due to the electrically conducing TiN layer), resulting in a fully activated Co_3O_4 layer. The two Co_3O_4 systems were biased at −50 V as magnetic hysteresis loops were continuously recorded. In Fig. 3(d), the evolution of the saturation magnetizations, M_S, for both systems is plotted as a function of time. While both systems show an increase in M_S, the capacitor configuration shows a near sixfold improvement in total magnetization (119 vs 700 emu cm^{-3}), indicating a much stronger magneto-ionic effect. Indeed, the *on* state in the capacitor configuration is activated faster than the transistor-like structure, with over a 35-fold improvement in magnetization rate (9 vs 325 memu cm^{-3} s^{-1}), showing that the biasing configuration plays a key role in the magneto-ionic performance of structural ion films. Aside from a much-improved magneto-ionic rate, the *on* state possesses a narrower H_C distribution [Fig. 3(e)], and the minimal onset threshold voltage is reduced (−4 vs −10 V), a direct consequence of the chosen configuration. The observed TEM and EELS images taken of lamellae cut from regions distant from the contact are in agreement,[152] showing a weakened ionic effect in the transistor-like configuration, although further examination would further illuminate the mechanisms at play, as analysis until now has not attempted to include dynamics. For example, TEM/EELS or VEPALS data taken for a series of exposure times, both near and far from the electrical contact, could provide further insight on how ions are distributed under bias using these configurations. While possessing mild activation rates, applications in neuromorphic and stochastic computing or magnetic MEMS are possible.[95] In addition, transition metal oxides, such as Co_3O_4, are relatively easy to grow in via reactive sputtering, making them well-suited for industrial applications.

To further extend the potential of the structural ion approach, an examination of the functionality of ions beyond oxygen in magneto-ionic target materials would likely prove fruitful. Indeed, we have shown that nitrogen[132,133] has significant advantages, both energetically and functionally, over their oxygen-based counterparts. Nitrogen[133] magneto-ionics was first observed in paramagnetic, polycrystalline CoN sputtered onto a Cu/Ti buffer layer that was biased much in the same way as the above Co_3O_4, using PC with solvated Na^+ ions to electrolyte-gate the films at -50 V while measuring M vs H loops. In Fig. 4(a), M_S is shown as a function of time, where the magneto-ionic rate of CoN is clearly much higher than Co_3O_4 films of the same thickness sputtered on identical substrates. M_S increases with time, asymptotically, reaching 588 emu cm^{-3} for Co_3O_4 and 637 emu cm^{-3} for CoN. The linear magnetization rate of CoN is calculated to be 722 memu cm^{-3} s^{-1}, a fivefold enhancement over sputtered Co_3O_4. However, it should be emphasized that this value may be considerably underestimated; the measurement device (VSM) is limited to measurements on the order of 10^{-7} emu and 10^{-1} s, so any assessment of set and reset events should be taken as a rough approximation. These promising results suggest that perhaps other transition metal nitrides,[153] such as the Fe–N system,[154] are also potential magneto-ionic candidates with built-in industrial qualities, including high hardness, melting point, and tunability of properties with nitrogen concentration. Indeed, a study on polycrystalline iron nitrides[132] reveals the viability of FeN; M_S as a function of time is presented in Fig. 4(a) alongside CoN. Interestingly, FeN exhibits a distinct multistep process, with M_S initially increasing at a rate slower than CoN but faster than Co_3O_4, attributed to the appearance of a Fe_3N phase, and then slowing down and reaching a maximum M_S of 898 emu cm^{-3}, i.e., higher than CoN. Perhaps the most interesting feature of nitrogen magneto-ionics, beyond the increased magneto-ionic rates, is the exact *way* in which the ions are transported from the film. An examination of the films after biasing at -50 V using TEM and EELS gave a fascinating insight as to how the different anions move through the films [Fig. 4(b)]. After biasing at −50 V, the Co_3O_4 film redistributes oxygen into irregular O-rich channels, similar to that seen in Fig. 3(b). However, in CoN, a well-defined, planar interface parallel to the surface is observed, dividing the film in two sublayers with two distinct microstructures. No nitrogen is detected in either of the two sublayers, escaping beyond the film and into the electrolyte. Sublayer 1 (near the electrolyte) is found to be amorphous-like and less dense, while sublayer 2 (near the electrode) is highly nanocrystalline. A similar, although somewhat rougher, sublayer structure is observed in FeN, reflected in the homogeneous distribution of atomic Fe and N near the working electrode and a reduced amount of N atoms near the electrolyte side, consistent with the formation of Fe_3N. To understand if this planar migration front is consistent through the voltage range and perhaps correlated with defect structure, variable energy positron annihilation lifetime spectroscopy experiments for CoN were performed and results are shown in Fig. 4(c).[132,133] For simplicity, only the intensity (I_2) of lifetime τ_2, corresponding to the density of defects in the form of surface states and grain boundaries, is shown. A monotonic increase in relative intensity I_2 is found in the as-prepared CoN, whereas relative jumps are found for the treated CoN films (highlighted in yellow). The depth position of these relative maxima increases with the applied voltage (−20 to −50 V), confirming the occurrence of a planar migration front, in agreement with TEM observations. The ionic transport upon electrolyte-gating in CoN is, thus, consistent with a uniform nitrogen migration through vacancies and grain boundaries, leaving behind a larger density of grain boundaries. Although not shown here, a migration front is also observed in FeN,[132] even under the minimal bias needed to activate ionic motion (onset voltage). It must be noted here that this planar front is a unique

© Author(s) 2022

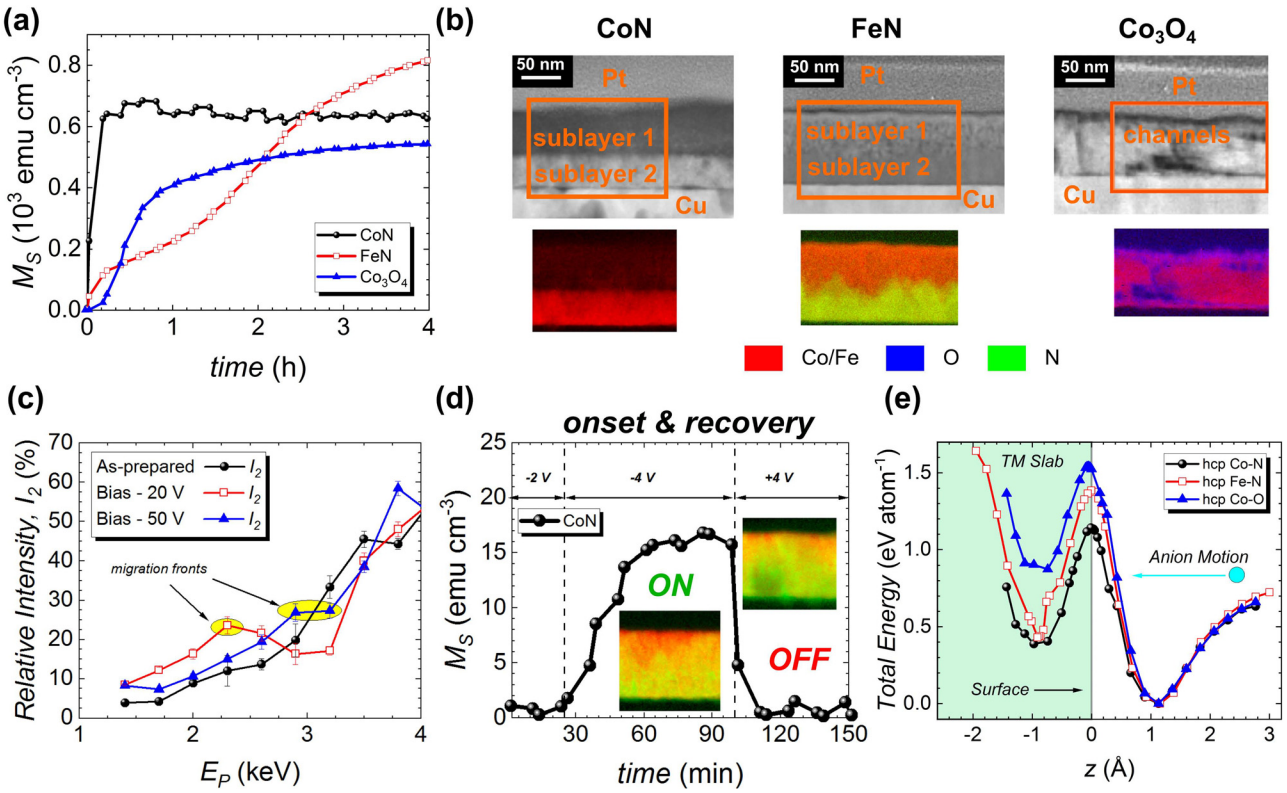

FIG. 4. (a) Evolution of the saturation magnetization as a function of time (M_S vs t) for CoN, FeN, and Co_3O_4 films. (b) HAADF-STEM images and corresponding elemental EELS mappings of the areas marked in orange, of the CoN, FeN, and Co_3O_4 films subjected to a −50 V for 75 min. Colors corresponding to each element are shown just below the figure. (c) Positron lifetime relative intensity I_2 (corresponding to grain boundaries) as a function of positron implantation energy E_p for as-prepared, −20, and −50 V biased CoN films. Relative peaks in intensity of I_2 correspond to the position of the moving planar migration front between Co sublayers, highlighted in yellow. (d) Evolution of M_S as voltage is increased in steps of −2 V to determine the onset and recovery voltages. Insets show EELS mappings after *on* and *off* switching. (e) Calculated total energy per atom, normalized to the minimum energy value, as a function of the position of the inserted ion relative to the surface. The black circles, red squares, and blue triangles correspond to the Co–N, Fe–N, and Co–O energetic paths, respectively. Adapted with permission from de Rojas *et al.*, Nat. Commun. **11**, 5871 (2020). Copyright 2020 Springer Nature. Adapted with permission from de Rojas *et al.*, ACS Appl. Mater. Interfaces **13**(26) 30826–30834 (2021). Copyright 2021 American Chemical Society.

trait, one which can be imagined to allow the imprinting of magnetic shapes parallel to the applied field, and potentially allowing for the toggling of related magnetic and stoichiometrically controlled crystalline states. This planar front is currently attributed[131] to the highly nanostructured nature of the films, isotropic grains, and a defect gradient along the depth of the film, with more defects near the top and fewer near the working electrode, resulting in faster ionic motion occurring near the surface under voltage, while relatively fewer defects result in lower ionic rates deeper in the film. This, along with the smaller, isotropic grains compared with Co_3O_4 and lower electrical resistivity effectively makes the ionic front penetration depth a voltage dependent quantity. While CoN does generate magnetic phase faster than FeN and with a more clearly defined planar front, the generated ferromagnetic phases possess different hysteresis loop shapes. In general, iron nitride films show a larger increase in coercive field, H_C, up to $\approx 10^2$ Oe, compared with $\approx 10^1$ Oe in cobalt nitride, indicative of relatively smaller activated magnetic regions, comprising single- or few-domain structures in mostly denitrided regions. This suggests that FeN, while slower, may be more useful for magnetic memory applications. The energy required to set a magnetic state was evaluated by an onset and reset process, shown in Fig. 4(d). Not only is the onset voltage for CoN (−4 V) found to be lower than that for Co_3O_4, but it also recovers the paramagnetic state under biasing at +4 V (for Co_3O_4 a larger positive voltage is required). The insets of Fig. 4(d) show EELS images of the CoN film during the onset and recovery processes, revealing that under −4 V biasing, CoN develops a slightly nanoporous structure and a decrease in the nitrogen content near the electrolyte, while, after +4 V biasing, the film is nearly fully recovered with very small nitrogen-deficient regions. This polarization symmetry is a distinct advantage of N^{3-} over O^{2-}, which requires asymmetric biasing to recover the original state (i.e., a positive bias of +20 V must be applied to recover a sample biased at −6 V). Similar results are observed in FeN, where complete recovery is achieved under equivalent positive biasing. To understand this difference between oxygen and nitrogen, formation energies of Co–O, Co–N, and Fe–N, shown in Fig. 4(e), were calculated by determining minimum energy paths of N inserted into a transition metal slab, plotted as a function of the position of the oxygen or nitrogen relative to the surface (reflective of an *on-off* transition). The critical electric field needed to induce oxygen or nitrogen motion can be estimated by $E_C = \Delta V/\Delta z$, where ΔV is the

© Author(s) 2022

electric potential per atom to overcome the energy barrier and Δz is the distance between minima. This critical field is found to be $\approx$8.1 V nm^{-1} for Co_3O_4, $\approx$6.6 V nm^{-1} for FeN, and $\approx$5.3 V nm^{-1} CoN, in agreement with the observed onset voltages. Although the crystallographic structures of CoN, FeN, and Co_3O_4 were not exactly reproduced in the modeling, it is still a reasonable approximation of an *off-on* process in a polycrystalline film. These results complement recent calculations, which show that CoN has a lower energy barrier compared to Co_3O_4 as well as previous simulations where CoN was found to have a lower cohesive energy than FeN.[155,156] Nitrogen magneto-ionics, thus far, presents a desirable blend of qualities as a magneto-ionic anion, such as requiring lower activation voltages, higher cyclability (under symmetric bias), much faster rates of motion and, perhaps most interestingly, a planar ionic motion front that generates a voltage-programmable ion depth profile, potentially allowing for the nonvolatile imprinting and destruction of magnetic sublayers. These features, such as the voltage-tunable analog changes in M_S [Fig. 4d)], may open the door to an eventual utilization of magneto-ionics in neuromorphic applications. Remarkably, the magnetic signals described here rely on voltage-driven oxygen or nitrogen ion migration, much like ion channels activated with electric stimuli in neurons' membranes in the brain.

Extending magneto-ionic targets with structural-ions toward device viability require tackling several hurdles, including the effect of dimensional reduction and patterning. As a preview, initial steps toward "imprinting" a magnetic region into a structural-ion target under biasing are shown for a 100 nm thick, polycrystalline Co_3O_4 film sputtered onto a Cu/Ti/SiO_2 substrate. Cu stripes were then patterned atop the Co_3O_4 film, leaving only the exposed (uncovered) Co_3O_4 regions in contact with PC during biasing. The Cu stripes were fabricated by photolithography using a photoresist of stripes with dimensions of 2.4 mm $\times$ 5 μm and a pitch of 12 μm, atop which a 100 nm thick Cu layer was then sputtered. Once the photoresist was lifted off, alternating Cu and exposed Co_3O_4 stripes were left behind, constituting 45% of the area, as shown in Fig. 5(a). We have assigned directionality to the stripes on the film, with 0° corresponding to the direction parallel to the lines, and 90° corresponding to the direction perpendicular to the lines. Once again using PC, the samples were

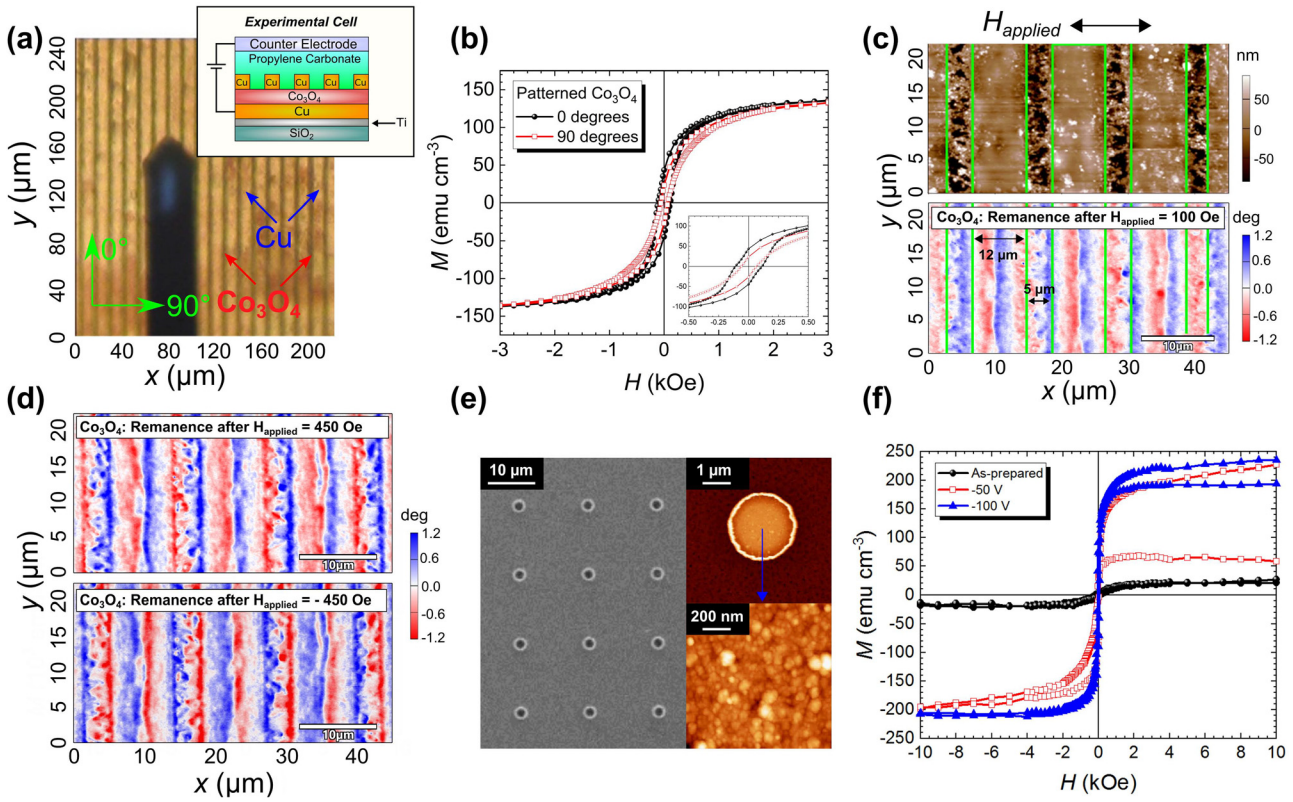

FIG. 5. (a) Image of the patterned Co_3O_4 film with a Cu mask. Dark stripes correspond to exposed Co_3O_4, light stripes correspond to the Cu mask. Inset is a schematic of the film and electrical circuit used for measurements shown in (a)–(d). Directions parallel and perpendicular to the exposed Co_3O_4 regions are noted 0° and 90°, respectively. (b) Normalized magnetic moment, M, vs applied magnetic field, H, of Co_3O_4 after treatment at −50 V for 75 min, measured along both the 0° and 90° directions, with asymmetry reflecting the emergence of hard and easy axes. (c) Atomic force microscopy (AFM, top) and magnetic force microscopy (MFM, bottom) measured at (non-saturated) remanence after an applied external field of 100 Oe was applied along 90°. Green lines are provided as guides to the eye marking the outline of the Cu mask. (d) MFM measurements at remanence after an applied external field of 450 Oe (top) and −450 Oe (bottom) were directed along 90°, showing greater magnetic contrast. (e) AFM measurements of 2 μm radius FeN dots grown onto a Cu/Ti buffer layer. (f) Normalized magnetic moment, M, vs applied magnetic field, H, of FeN dots after sequential treatment at −50 and −100 V, for 25 min each, measured in plane.

© Author(s) 2022

biased at −50 V for 75 min, with hysteresis loops measured by VSM post-biasing. Biasing not only results in magneto-ionic effects in the exposed Co_3O_4 stripes but, to a lesser extent, also below the Cu lines, results in a well-defined patterned magnetic composite. The patterns even exhibit a magnetic shape anisotropy depending on the measurement direction, as seen in Fig. 5(b), a feature not seen in treated samples without patterned Cu stripes. This confirms a magneto-ionic generation of magnetic anisotropy. Here, the hard-axis is found to be along the stripe short axis (90°), consistent with a hard axis due to shape anisotropy perpendicular to the stripe long axis, while the easy axis direction, 0°, is consistent with shape anisotropy observed parallel to the stripe long axis, suggesting that the observed hard and easy axes are the result of selectively activating Co_3O_4 regions due to the Cu mask. To further explore the magnetic imprinting achieved in the film, atomic force microscopy (AFM) and magnetic force microscopy (MFM) measurements were performed, as shown in Fig. 5(c). The topography by AFM (top figure) shows the masked film, with the broader, lighter color corresponding to the Cu mask, and the darker regions corresponding to the exposed, underlying Co_3O_4. The magnetic profiling by MFM (bottom figure) shows the MFM signal as measured at (non-saturated) remanence after applying an external magnetic field of 100 Oe to the film. A stripe pattern can be identified along the 0° direction, with clear magnetic domain structure whose sizes match the width of the exposed vs Cu-masked regions, confirming the generation of a well-defined patterned magnetic composite (due to the dissimilar magneto-ionic strengths in the non-masked and masked regions of the Co_3O_4 film). These stripes are even more pronounced under higher applied field (−450 and 450 Oe), shown in Fig. 5(d), with excellent demarcation of the exposed Co_3O_4. To aid in visualizing the evolution of the magnetic domains under an applied field, a movie is provided in the supplementary material. Along the same vein, nitrogen magneto-ionics has also been demonstrated on 125 nm thick polycrystalline FeN reactively sputtered onto a Ti/Cu substrate, subsequently masked using electron beam lithography patterning to obtain dots of 2 μm in radius with a pitch of 10 μm. Figure 5(e) shows the resulting FeN dots, which exhibit a clear ferromagnetic-*on* state when the dots were biased at −50 V for 75 min, with hysteresis loops measured by VSM after biasing was complete [Fig. 5(f)] the first demonstration of magneto-ionics in a patterned nitrogen magneto-ionic target.

Magneto-ionics research in the past few recent years has opened a plethora of possible materials chemistry, structure types, and magnetic states to be explored. Perhaps the most glaring involves operational speeds, durability, industrial deployment, and establishing functionalities (such as plasticity in neuromorphic computing). Many systems suffer from slow room-temperature ionic response ($\approx 10^2$–10^3 s) and are typically boosted via heating to induce ionic motion (at the expense of energy efficiency) in the range of 10^{-1} s or below,[82,84,143,157] which is much slower than current transistor flip speeds ($\lesssim 10^{-10}$ s), although proton-based systems are pushing switching times down to the order of 1 ms or lower.[81,123,124,135] In the structural ion systems discussed so far in this Perspective, switching speeds and cyclability must be addressed before they can be considered competitive with other magneto-ionic approaches. Switching states in structural ion systems require 10^2–10^3 s at room temperature, well behind H^+ or heat-assisted O^{2-} systems. Due to the reduction of energy efficiency when applying heat treatment to improve ionic motion, alternate approaches have been considered to reduce switching speeds. The structural ion films studied so far have been relatively thick when compared to other approaches (≈50–100 nm). Very recent work on oxide thin films[97] and an upcoming work on nitride thin films[158] with reduced thicknesses (≤25 nm) have demonstrated switching speeds <10 s for oxygen ion motion and <1 s for nitrogen ion motion. To achieve speeds of 1 ms or faster, however, additional work must be done, such as further microstructure tuning by, for instance, defect engineering through ion irradiation[159] and/or miniaturization by micro-/nanofabrication to promote surface diffusion over bulk diffusion since the latter results in faster ion mobility.[160] Moreover, in order to expand technological applications, other forms of the dielectric layer used to bias the films should be considered. Up to now, the structural-ion films discussed have been biased using a liquid electrolyte, a common and convenient biasing tool. The massive electric fields achieved via EDL formation are excellent for fundamental research, as is the relative ease of use (compared with sputtering a solid-state ionic conductor) and ability to apply biasing in exotic motifs outside thin films (foams, nanoporous materials, pillars, etc.). However, in order to move toward device applicability, solid state heterostructures using a dielectric sublayer to gate the films will be necessary. The fastest room temperature switching in oxygen-based systems has reached speeds up to 0.2 ms,[80] utilizing the very high oxygen mobility in $SrCoO_{2.5}$ to produce limited but measurable interfacial interactions, an indication that properly tuned dielectrics can have a huge impact on ionic migration. Generally speaking, progress via hydrogen boosting, as seen in GdO_x,[123] and battery-like intercalation can be promising,[130,134] while in the specific case of nitrogen magneto-ionics solid state structures will require exploring possible nitrogen reservoir sources[161] (such as zirconium oxide-, tantalum oxide-, or mayenite-based nitrides, or GdN_x) that can assist the insertion and extraction of nitrogen ions from transition metal nitride layers.

In terms of durability, state-of-the-art magneto-ionic materials have shown high quality repeatability well over 1000 cycles,[81,124] while O^{2-} systems, including structural ion, have demonstrated 100 cycles or less. This can partly be attributed to the deformation or changes introduced when inducing ionic motion beyond the interface and may point toward three-dimensional, high surface-to-volume ratio structures focusing on interfacial effects being a more practical option. However, tailoring ionic pathways by, for example, ion irradiation of the target films may allow for more facile insertion and extraction of ions, improving durability and ionic rates. This can be done not only with He, Ar, or Xe ions (inert ions) but also by the same magneto-ionic ion species, such as O^{2-} or N^{3-}. This process is known to allow for tuning of structural defects and may affect ionic pathways and the electric field generated inside the target material.[131] The structural ion approach allows for tuning ion vacancies or enriching regions of the target material and consequently modifying magneto-ionic performance, as recently demonstrated by Jensen *et al.* in Gd/NiCoO.[162] Indeed, structural ion materials are still far from being fully optimized. The threshold voltage needed to actuate nonvolatile *on-off* behavior is ±4 V in CoN and ±8 V in Co_3O_4, comparable with voltages applied in other systems as can be found in a recent Perspective by Gu *et al.*,[163] although −50 V was needed to extract nitrogen up to a depth of 40 nm in relatively thick films. However, while several studied systems have required an asymmetric voltage to recover the pristine state and, in many cases, the phase transformations are irreversible, our

© Author(s) 2022

work has demonstrated that symmetric and recoverable states can be achieved in transition metal-nitride systems, suggesting that there is still more to learn about these systems. In particular, recent works have shown that DC voltage pulsing at frequencies in the range of 1–100 Hz results in cumulative magnet-ionic effects,[97,158] allowing for the frequency-dependent tuning of magnetic parameters, a path toward the neuromorphic applications of magneto-ionics, still in its infancy.[18,93] The observed dynamics under DC pulsing include a cumulative increase and partial recovery of magnetization (analogous to potentiation and depression), threshold activation, and spike-rate-dependent (i.e., frequency-dependent) magnetic plasticity for learning functionalities, giving access to functions seen in the biological synapse. Beyond ferromagnetic behavior, antiferromagnetic systems, such as or $Mn_xCo_{1-x}N$ or NiCoO, have yet to be exploited under magneto-ionic control at room temperature, and achieving *on-off* AFM toggling would represent a major step forward. Further dimensional scaling, as seen in the patterned lines and dots described above, or more exotic electrodeposited motifs, may provide a means by which to tune magnetic properties by the large-scale geometry of the system. Finally, considering the exotic phenomena exhibited by perovskite structures, the possibility of as-yet-unseen perovskite nitrides may open the possibility of complex nitride heterostructures with novel magnetic properties.[164]

In summary, recent research progress in magneto-ionics is overviewed, expanding to include a host of new magnetic materials, ions, and dielectrics in this rapidly-growing field. We presented our Perspective on what role structural-ion magneto-ionics and ionics beyond oxygen can play and highlighted the intriguing value of robust, fast, low-energy room-temperature *on-off* ferromagnetism using nitrogen magneto-ionics. Nitrogen magneto-ionics present a robust alternative for efficient voltage-driven effects and may enable the use of magneto-ionics in devices that require endurance and moderate speeds of operation, such as neuromorphic computing, magnetic MEMS, and MRAM, and perhaps promote the use of nitride semiconductors in fields, such as electrochemical sensors, catalysis, batteries, spintronics, or iontronics.

SUPPLEMENTARY MATERIAL

See the supplementary material for M–H loops after long-term storage of the nitride films (Fig. S1), extra MFM characterization (Fig. S2), and a movie (Fig. S3) of MFM imaging showing the evolution of magnetic domains as a function of an applied field for patterned Co_3O_4.

ACKNOWLEDGMENTS

Financial support by the European Research Council (SPINPORICS 2014-Consolidator Grant Agreement No. 648454, and the MAGIC-SWITCH 2019-Proof of Concept Grant, Agreement No. 875018), the Spanish Government (Nos. MAT2017-86357-C3-1-R, PDC2021-121276-C31, and PID2020-116844RB-C21), the Generalitat de Catalunya (2017-SGR-292 and 2018-LLAV-00032), and the European Regional Development Fund (Nos. MAT2017-86357-C3-1-R and 2018-LLAV-00032) were acknowledged. E.M. acknowledges support as a Serra Húnter Fellow. G.R. acknowledges support from Ayudas Ramon y Cajal No. RYC-2016-21412.

AUTHOR DECLARATIONS

Conflict of Interest

The authors declare no conflicts of interest.

DATA AVAILABILITY

The data that support the findings of this study are available from the corresponding authors upon reasonable request.

REFERENCES

[1]C. Mead, Proc. IEEE **78**, 1629 (1990).
[2]Y. LeCun, Y. Bengio, and G. Hinton, Nature **521**, 436 (2015).
[3]A. Krizhevsky, I. Sutskever, and G. E. Hinton, in *Proceedings of the 25th International Conference on Neural Information Processings Systems* (Curran Associates Inc., Red Hook, NY, 2012), Vol. 1, pp. 1097–1105.
[4]O. Vinyals, I. Babuschkin, W. M. Czarnecki, M. Mathieu, A. Dudzik, J. Chung, D. H. Choi, R. Powell, T. Ewalds, P. Georgiev, J. Oh, D. Horgan, M. Kroiss, I. Danihelka, A. Huang, L. Sifre, T. Cai, J. P. Agapiou, M. Jaderberg, A. S. Vezhnevets, R. Leblond, T. Pohlen, V. Dalibard, D. Budden, Y. Sulsky, J. Molloy, T. L. Paine, C. Gulcehre, Z. Wang, T. Pfaff, Y. Wu, R. Ring, D. Yogatama, D. Wünsch, K. McKinney, O. Smith, T. Schaul, T. Lillicrap, K. Kavukcuoglu, D. Hassabis, C. Apps, and D. Silver, Nature **575**, 350 (2019).
[5]H. Esmaeilzadeh, E. Blem, R. S. Amant, K. Sankaralingam, and D. Burger, in *38th Annual International. Symposium on Computer Architecture* (IEEE, 2011), pp. 365–376; available at https://ieeexplore.ieee.org/abstract/document/6307773.
[6]I. L. Markov, Nature **512**, 147 (2014).
[7]G. E. Moore, Electronics **38**, 114 (1965).
[8]I. Žutić, J. Fabian, and S. Das Sarma, Rev. Mod. Phys. **76**, 323 (2004).
[9]S. A. Wolf, D. D. Awschalom, R. A. Buhrman, J. M. Daughton, S. von Molnár, M. L. Roukes, A. Y. Chtchelkanova, and D. M. Treger, Science **294**, 1488 (2001).
[10]T. Kawahara, K. Ito, R. Takemura, and H. Ohno, Microelectron. Reliab. **52**, 613 (2012).
[11]A. Brataas, A. D. Kent, and H. Ohno, Nat. Mater. **11**, 372 (2012).
[12]X. Han, X. Wang, C. Wan, G. Yu, and X. Lv, Appl. Phys. Lett. **118**, 120502 (2021).
[13]P. Gambardella and I. M. Miron, Philos. Trans. R. Soc., A **369**, 3175 (2011).
[14]S. Lange, J. Pohl, and T. Santarius, Ecol. Econ. **176**, 106760 (2020).
[15]A. Andrae and T. Edler, Challenges **6**, 117 (2015).
[16]J. Fan, F. Han, and H. Liu, Natl. Sci. Rev. **1**, 293 (2014).
[17]C. Song, B. Cui, F. Li, X. Zhou, and F. Pan, Prog. Mater. Sci. **87**, 33 (2017).
[18]M. Nichterwitz, S. Honnali, M. Kutuzau, S. Guo, J. Zehner, K. Nielsch, and K. Leistner, APL Mater. **9**, 030903 (2021).
[19]C. Navarro-Senent, A. Quintana, E. Menéndez, E. Pellicer, and J. Sort, APL Mater. **7**, 030701 (2019).
[20]A. Molinari, H. Hahn, and R. Kruk, Adv. Mater. **31**, 1806662 (2019).
[21]F. Matsukura, Y. Tokura, and H. Ohno, Nat. Nanotechnol. **10**, 209 (2015).
[22]J. M. Hu and C. W. Nan, APL Mater. **7**, 080905 (2019).
[23]P. Curie, J. Phys. Théor. Appl. **3**, 393 (1894).
[24]P. Debye, Z. Phys. **36**, 300 (1926).
[25]L. D. Landau and E. M. Lifshitz, *Electrodynamics of Continuous Media*, 1st ed. (Addison-Wesley Publishing Company, Inc., Reading, MA, 1960).
[26]I. E. Dzyaloshinskii, J. Exp. Theor. Phys. **10**, 881 (1959).
[27]V. J. Folen, G. T. Rado, and E. W. Stalder, Phys. Rev. Lett. **6**, 607 (1961).
[28]D. N. Astrov, J. Exp. Theor. Phys. **11**, 708 (1960).
[29]D. N. Astrov, J. Exp. Theor. Phys. **13**, 729 (1961).
[30]G. T. Rado and V. J. Folen, Phys. Rev. Lett. **7**, 310 (1961).
[31]E. Ascher, H. Rieder, H. Schmid, and H. Stössel, J. Appl. Phys. **37**, 1404 (1966).
[32]S. V. Kiselev, R. P. Ozerov, and G. S. Zhdanov, Sov. Phys. Dokl. **7**, 742 (1963).
[33]S. Gnewuch and E. E. Rodriguez, J. Solid State Chem. **271**, 175 (2019).
[34]N. A. Hill, J. Phys. Chem. B **104**, 6694 (2000).
[35]N. A. Spaldin and M. Fiebig, Science **309**, 391 (2005).
[36]N. A. Spaldin and R. Ramesh, Nat. Mater. **18**, 203 (2019).
[37]M. Fiebig, T. Lottermoser, D. Meier, and M. Trassin, Nat. Rev. Mater. **1**, 16046 (2016).

© Author(s) 2022

[38]M. Fiebig, J. Phys. D: Appl. Phys. **38**, R123 (2005).
[39]W. Eerenstein, N. D. Mathur, and J. F. Scott, Nature **442**, 759 (2006).
[40]C. A. F. Vaz, J. Hoffman, C. H. Ahn, and R. Ramesh, Adv. Mater. **22**, 2900 (2010).
[41]S. Zhang, Y. G. Zhao, P. S. Li, J. J. Yang, S. Rizwan, J. X. Zhang, J. Seidel, T. L. Qu, Y. J. Yang, Z. L. Luo, Q. He, T. Zou, Q. P. Chen, J. W. Wang, L. F. Yang, Y. Sun, Y. Z. Wu, X. Xiao, X. F. Jin, J. Huang, C. Gao, X. F. Han, and R. Ramesh, Phys. Rev. Lett. **108**, 137203 (2012).
[42]F. Zavaliche, H. Zheng, L. Mohaddes-Ardabili, S. Y. Yang, Q. Zhan, P. Shafer, E. Reilly, R. Chopdekar, Y. Jia, P. Wright, D. G. Schlom, Y. Suzuki, and R. Ramesh, Nano Lett. **5**, 1793 (2005).
[43]T. Wu, A. Bur, K. Wong, P. Zhao, C. S. Lynch, P. K. Amiri, K. L. Wang, and G. P. Carman, Appl. Phys. Lett. **98**, 262504 (2011).
[44]J. Lou, M. Liu, D. Reed, Y. Ren, and N. X. Sun, Adv. Mater. **21**, 4711 (2009).
[45]M. Liu, O. Obi, J. Lou, S. Stoute, J. Y. Huang, Z. Cai, K. S. Ziemer, and N. X. Sun, Appl. Phys. Lett. **92**, 152504 (2008).
[46]M. Liu, O. Obi, J. Lou, Y. Chen, Z. Cai, S. Stoute, M. Espanol, M. Lew, X. Situ, K. S. Ziemer, V. G. Harris, and N. X. Sun, Adv. Funct. Mater. **19**, 1826 (2009).
[47]Y. Lee, Z. Q. Liu, J. T. Heron, J. D. Clarkson, J. Hong, C. Ko, M. D. Biegalski, U. Aschauer, S. L. Hsu, M. E. Nowakowski, J. Wu, H. M. Christen, S. Salahuddin, J. B. Bokor, N. A. Spaldin, D. G. Schlom, and R. Ramesh, Nat. Commun. **6**, 5959 (2015).
[48]T. Brintlinger, S. H. Lim, K. H. Baloch, P. Alexander, Y. Qi, J. Barry, J. Melngailis, L. Salamanca-Riba, I. Takeuchi, and J. Cumings, Nano Lett. **10**, 1219 (2010).
[49]A. M. J. G. Van Run, D. R. Terrell, and J. H. Scholing, J. Mater. Sci. **9**, 1710 (1974).
[50]J. Van Den Boomgaard, D. R. Terrell, R. A. J. Born, and H. F. J. I. Giller, J. Mater. Sci. **9**, 1705 (1974).
[51]H. Ohno, D. Chiba, F. Matsukura, T. Omiya, E. Abe, T. Dietl, Y. Ohno, and K. Ohtani, Nature **408**, 944 (2000).
[52]D. Chiba, H. Yamanouchi, F. Matsukura, and H. Ohno, Science **301**, 943 (2003).
[53]D. Chiba, F. Matsukura, and H. Ohno, Nano Lett. **10**, 4505 (2010).
[54]M. Sawicki, D. Chiba, A. Korbecka, Y. Nishitani, J. A. Majewski, F. Matsukura, T. Dietl, and H. Ohno, Nat. Phys. **6**, 22 (2010).
[55]M. Endo, S. Kanai, S. Ikeda, F. Matsukura, and H. Ohno, Appl. Phys. Lett. **96**, 212503 (2010).
[56]C. G. Duan, J. P. Velev, R. F. Sabirianov, Z. Zhu, J. Chu, S. S. Jaswal, and E. Y. Tsymbal, Phys. Rev. Lett. **101**, 137201 (2008).
[57]D. Chiba, S. Fukami, K. Shimamura, N. Ishiwata, K. Kobayashi, and T. Ono, Nat. Mater. **10**, 853 (2011).
[58]T. Maruyama, Y. Shiota, T. Nozaki, K. Ohta, N. Toda, M. Mizuguchi, A. A. Tulapurkar, T. Shinjo, M. Shiraishi, S. Mizukami, Y. Ando, and Y. Suzuki, Nat. Nanotechnol. **4**, 158 (2009).
[59]M. Weisheit, S. Fähler, A. Marty, Y. Souche, C. Poinsignon, and D. Givord, Science **315**, 349 (2007).
[60]C. A. F. Vaz, J. Hoffman, Y. Segal, J. W. Reiner, R. D. Grober, Z. Zhang, C. H. Ahn, and F. J. Walker, Phys. Rev. Lett. **104**, 127202 (2010).
[61]H. J. A. Molegraaf, J. Hoffman, C. A. F. Vaz, S. Gariglio, D. van der Marel, C. H. Ahn, and J.-M. Triscone, Adv. Mater. **21**, 3470 (2009).
[62]A. J. Grutter, B. J. Kirby, M. T. Gray, C. L. Flint, U. S. Alaan, Y. Suzuki, and J. A. Borchers, Phys. Rev. Lett. **115**, 047601 (2015).
[63]F. Bi, M. Huang, S. Ryu, H. Lee, C. W. Bark, C. B. Eom, P. Irvin, and J. Levy, Nat. Commun. **5**, 5019 (2014).
[64]S. R. Spurgeon, P. V. Balachandran, D. M. Kepaptsoglou, A. R. Damodaran, J. Karthik, S. Nejati, L. Jones, H. Ambaye, V. Lauter, Q. M. Ramasse, K. K. S. Lau, L. W. Martin, J. M. Rondinelli, and M. L. Taheri, Nat. Commun. **6**, 6735 (2015).
[65]S. M. Wu, S. A. Cybart, P. Yu, M. D. Rossell, J. X. Zhang, R. Ramesh, and R. C. Dynes, Nat. Mater. **9**, 756 (2010).
[66]V. Skumryev, V. Laukhin, I. Fina, X. Martí, F. Sánchez, M. Gospodinov, and J. Fontcuberta, Phys. Rev. Lett. **106**, 057206 (2011).
[67]V. Laukhin, V. Skumryev, X. Martí, D. Hrabovsky, F. Sánchez, M. V. García-Cuenca, C. Ferrater, M. Varela, U. Lüders, J. F. Bobo, and J. Fontcuberta, Phys. Rev. Lett. **97**, 227201 (2006).
[68]X. He, Y. Wang, N. Wu, A. N. Caruso, E. Vescovo, K. D. Belashchenko, P. A. Dowben, and C. Binek, Nat. Mater. **9**, 579 (2010).
[69]S. Dong, K. Yamauchi, S. Yunoki, R. Yu, S. Liang, A. Moreo, J.-M. Liu, S. Picozzi, and E. Dagotto, Phys. Rev. Lett. **103**, 127201 (2009).
[70]Y. H. Chu, L. W. Martin, M. B. Holcomb, M. Gajek, S. J. Han, Q. He, N. Balke, C. H. Yang, D. Lee, W. Hu, Q. Zhan, P. L. Yang, A. Fraile-Rodríguez, A. Scholl, S. X. Wang, and R. Ramesh, Nat. Mater. **7**, 478 (2008).
[71]B. Cui, C. Song, H. Mao, Y. Yan, F. Li, S. Gao, J. Peng, F. Zeng, and F. Pan, Adv. Funct. Mater. **26**, 753 (2016).
[72]Y. Tokura and N. Nagaosa, Science **288**, 462 (2000).
[73]D. Preziosi, M. Alexe, D. Hesse, and M. Salluzzo, Phys. Rev. Lett. **115**, 157401 (2015).
[74]J. Garcia-Barriocanal, J. C. Cezar, F. Y. Bruno, P. Thakur, N. B. Brookes, C. Utfeld, A. Rivera-Calzada, S. R. Giblin, J. W. Taylor, J. A. Duffy, S. B. Dugdale, T. Nakamura, K. Kodama, C. Leon, S. Okamoto, and J. Santamaria, Nat. Commun. **1**, 82 (2010).
[75]C. G. Duan, S. S. Jaswal, and E. Y. Tsymbal, Phys. Rev. Lett. **97**, 047201 (2006).
[76]J. Chakhalian, J. W. Freeland, H. U. Habermeier, G. Cristiani, G. Khaliullin, M. Van Veenendaal, and B. Keimer, Science **318**, 1114 (2007).
[77]J. Q. Dai, H. Zhang, and Y. M. Song, J. Magn. Magn. Mater. **324**, 3937 (2012).
[78]X. Zhou, Y. Yan, M. Jiang, B. Cui, F. Pan, and C. Song, J. Phys. Chem. C **120**, 1633 (2016).
[79]Y. N. Yan, X. J. Zhou, F. Li, B. Cui, Y. Y. Wang, G. Y. Wang, F. Pan, and C. Song, Appl. Phys. Lett. **107**, 122407 (2015).
[80]H. B. Li, N. Lu, Q. Zhang, Y. Wang, D. Feng, T. Chen, S. Yang, Z. Duan, Z. Li, Y. Shi, W. Wang, W. H. Wang, K. Jin, H. Liu, J. Ma, L. Gu, C. Nan, and P. Yu, Nat. Commun. **8**, 2156 (2017).
[81]K.-Y. Y. Lee, S. Jo, A. J. Tan, M. Huang, D. Choi, J. H. Park, H.-I. Il Ji, J.-W. W. Son, J. Chang, G. S. D. D. Beach, and S. Woo, Nano Lett. **20**, 3435 (2020).
[82]D. A. Gilbert, A. J. Grutter, E. Arenholz, K. Liu, B. J. Kirby, J. A. Borchers, and B. B. Maranville, Nat. Commun. **7**, 12264 (2016).
[83]C. Bi, Y. Liu, T. Newhouse-Illige, M. Xu, M. Rosales, J. W. Freeland, O. Mryasov, S. Zhang, S. G. E. Te Velthuis, and W. G. Wang, Phys. Rev. Lett. **113**, 267202 (2014).
[84]U. Bauer, L. Yao, A. J. Tan, P. Agrawal, S. Emori, H. L. Tuller, S. Van Dijken, and G. S. D. Beach, Nat. Mater. **14**, 174 (2015).
[85]M. Jiang, X. Z. Chen, X. J. Zhou, B. Cui, Y. N. Yan, H. Q. Wu, F. Pan, and C. Song, Appl. Phys. Lett. **108**, 202404 (2016).
[86]A. J. Schellekens, A. van den Brink, J. H. Franken, H. J. M. Swagten, and B. Koopmans, Nat. Commun. **3**, 847 (2012).
[87]J. Walter, H. Wang, B. Luo, C. D. Frisbie, and C. Leighton, ACS Nano **10**, 7799 (2016).
[88]Y. Yamada, K. Ueno, T. Fukumura, H. T. Yuan, H. Shimotani, Y. Iwasa, L. Gu, S. Tsukimoto, Y. Ikuhara, and M. Kawasaki, Science **332**, 1065 (2011).
[89]J. Walter, B. Voigt, E. Day-Roberts, K. Heltemes, R. M. Fernandes, T. Birol, and C. Leighton, Sci. Adv. **6**, 7721 (2020).
[90]J. Zehner, I. Soldatov, S. Schneider, R. Heller, N. B. Khojasteh, S. Schiemenz, S. Fähler, K. Nielsch, R. Schäfer, and K. Leistner, Adv. Electron. Mater. **6**, 2000406 (2020).
[91]D. Yi, Y. Wang, O. M. J. van 't Erve, L. Xu, H. Yuan, M. J. Veit, P. P. Balakrishnan, Y. Choi, A. T. N'Diaye, P. Shafer, E. Arenholz, A. Grutter, H. Xu, P. Yu, B. T. Jonker, and Y. Suzuki, Nat. Commun. **11**, 902 (2020).
[92]K. Taniguchi, K. Narushima, H. Sagayama, W. Kosaka, N. Shito, and H. Miyasaka, Adv. Funct. Mater. **27**, 1604990 (2017).
[93]R. Mishra, D. Kumar, and H. Yang, Phys. Rev. Appl. **11**, 054065 (2019).
[94]K. Leistner, J. Wunderwald, N. Lange, S. Oswald, M. Richter, H. Zhang, L. Schultz, and S. Fähler, Phys. Rev. B **87**, 224411 (2013).
[95]C. Leighton, Nat. Mater. **18**, 13 (2019).
[96]K. Duschek, D. Pohl, S. Fähler, K. Nielsch, and K. Leistner, APL Mater. **4**, 032301 (2016).
[97]S. Martins, J. de Rojas, Z. Tan, M. Cialone, A. Lopeandia, J. Herrero-Martín, J. L. Costa-Krämer, E. Menéndez, and J. Sort, Nanoscale **14**, 842 (2022).
[98]N. D'Souza, M. S. Fashami, S. Bandyopadhyay, and J. Atulasimha, Nano Lett. **16**, 1069 (2016).
[99]S. Manipatruni, D. E. Nikonov, C. C. Lin, T. A. Gosavi, H. Liu, B. Prasad, Y. L. Huang, E. Bonturim, R. Ramesh, and I. A. Young, Nature **565**, 35 (2019).

© Author(s) 2022

[100]X. Li, A. Lee, S. A. Razavi, H. Wu, and K. L. Wang, MRS Bull. **43**, 970 (2018).
[101]J. Lee and W. D. Lu, Adv. Mater. **30**, 1702770 (2018).
[102]Z. Luo, Z. Lu, C. Xiong, T. Zhu, W. Wu, Q. Zhang, H. Wu, X. Zhang, and X. Zhang, Adv. Mater. **29**, 1605027 (2017).
[103]C. Navau and J. Sort, APL Mater. **9**, 070903 (2021).
[104]S. Sundaram, M. Skouras, D. S. Kim, L. van den Heuvel, and W. Matusik, Sci. Adv. **5**, eaaw1160 (2019).
[105]J. Rahmer, C. Stehning, and B. Gleich, Sci. Rob. **2**, eaal2845 (2017).
[106]J. Kim, S. E. Chung, S. E. Choi, H. Lee, J. Kim, and S. Kwon, Nat. Mater **10**, 747 (2011).
[107]L. A. Dubraja, C. Reitz, L. Velasco, R. Witte, R. Kruk, H. Hahn, and T. Brezesinski, ACS Appl. Nano Mater. **1**, 65 (2018).
[108]M. A. McEvoy and N. Correll, Science **347**, 1261689 (2015).
[109]Y. Yan, C. Wan, X. Zhou, G. Shi, B. Cui, J. Han, Y. Fan, X. Han, K. L. Wang, F. Pan, and C. Song, Adv. Electron. Mater. **2**, 1600219 (2016).
[110]X. Chen, C. Feng, Z. L. Wu, F. Yang, Y. Liu, S. Jiang, M. H. Li, and G. H. Yu, Appl. Phys. Lett. **104**, 052413 (2014).
[111]S. Ikeda, K. Miura, H. Yamamoto, K. Mizunuma, H. D. Gan, M. Endo, S. Kanai, J. Hayakawa, F. Matsukura, and H. Ohno, Nat. Mater. **9**, 721 (2010).
[112]D. A. Gilbert, B. B. Maranville, A. L. Balk, B. J. Kirby, P. Fischer, D. T. Pierce, J. Unguris, J. A. Borchers, and K. Liu, Nat. Commun. **6**, 8462 (2015).
[113]S. Mühlbauer, B. Binz, F. Jonietz, C. Pfleiderer, A. Rosch, A. Neubauer, R. Georgii, and P. Böni, Science **323**, 915 (2009).
[114]Z. Luo, T. P. Dao, A. Hrabec, J. Vijayakumar, A. Kleibert, M. Baumgartner, E. Kirk, J. Cui, T. Savchenko, G. Krishnaswamy, L. J. Heyderman, and P. Gambardella, Science **363**, 1435 (2019).
[115]G. Chen, J. Zhu, A. Quesada, J. Li, A. T. N'Diaye, Y. Huo, T. P. Ma, Y. Chen, H. Y. Kwon, C. Won, Z. Q. Qiu, A. K. Schmid, and Y. Z. Wu, Phys. Rev. Lett. **110**, 177204 (2013).
[116]M. Bode, M. Heide, K. Von Bergmann, P. Ferriani, S. Heinze, G. Bihlmayer, A. Kubetzka, O. Pietzsch, S. Blügel, and R. Wiesendanger, Nature **447**, 190 (2007).
[117]M. Hervé, B. Dupé, R. Lopes, M. Böttcher, M. D. Martins, T. Balashov, L. Gerhard, J. Sinova, and W. Wulfhekel, Nat. Commun. **9**, 1015 (2018).
[118]G. Chen, M. Robertson, M. Hoffmann, C. Ophus, A. L. F. Cauduro, R. Lo Conte, H. Ding, R. Wiesendanger, S. Blügel, A. K. Schmid, and K. Liu, Phys. Rev. X **11**, 021015 (2021).
[119]G. Chen, A. Mascaraque, H. Jia, B. Zimmermann, M. Robertson, R. Lo Conte, M. Hoffmann, M. A. G. Barrio, H. Ding, R. Wiesendanger, E. G. Michel, S. Blügel, A. K. Schmid, and K. Liu, Sci. Adv. **6**, eaba4924 (2020).
[120]T. Koyama, Y. Nakatani, J. Ieda, and D. Chiba, Sci. Adv. **4**, aav0265 (2018).
[121]T. Srivastava, M. Schott, R. Juge, V. Křižáková, M. Belmeguenai, Y. Roussigné, A. Bernand-Mantel, L. Ranno, S. Pizzini, S. M. Chérif, A. Stashkevich, S. Auffret, O. Boulle, G. Gaudin, M. Chshiev, C. Baraduc, and H. Béa, Nano Lett. **18**, 4871 (2018).
[122]F. Trier, P. Noël, J. Von Kim, J. P. Attané, L. Vila, and M. Bibes, Nat. Rev. Mater. (published online, 2021).
[123]A. J. Tan, M. Huang, S. Sheffels, F. Büttner, S. Kim, A. H. Hunt, I. Waluyo, H. L. Tuller, and G. S. D. Beach, Phys. Rev. Mater. **3**, 064408 (2019).
[124]A. J. Tan, M. Huang, C. O. Avci, F. Büttner, M. Mann, W. Hu, C. Mazzoli, S. Wilkins, H. L. Tuller, and G. S. D. Beach, Nat. Mater. **18**, 35 (2019).
[125]J. Zehner, D. Wolf, M. U. Hasan, M. Huang, D. Bono, K. Nielsch, K. Leistner, and G. S. D. Beach, Phys. Rev. Mater. **5**, L061401 (2021).
[126]X. Zhu, J. Zhou, L. Chen, S. Guo, G. Liu, R. W. Li, and W. D. Lu, Adv. Mater. **28**, 7658 (2016).
[127]Q. Zhang, X. Luo, L. Wang, L. Zhang, B. Khalid, J. Gong, and H. Wu, Nano Lett. **16**, 583 (2016).
[128]S. Dasgupta, B. Das, Q. Li, D. Wang, T. T. Baby, S. Indris, M. Knapp, H. Ehrenberg, K. Fink, R. Kruk, and H. Hahn, Adv. Funct. Mater. **26**, 7507 (2016).
[129]S. Dasgupta, B. Das, M. Knapp, R. A. Brand, H. Ehrenberg, R. Kruk, and H. Hahn, Adv. Mater. **26**, 4639 (2014).
[130]G. Wei, L. Wei, D. Wang, Y. Chen, Y. Tian, S. Yan, L. Mei, and J. Jiao, Appl. Phys. Lett. **110**, 062404 (2017).
[131]J. de Rojas, J. Salguero, A. Quintana, A. Lopeandia, M. O. Liedke, M. Butterling, A. G. Attallah, E. Hirschman, A. Wagner, L. Abad, J. L. Costa-Krämer, J. Sort, and E. Menéndez, Phys. Rev. Appl. **16**, 034042 (2021).
[132]J. de Rojas, J. Salguero, F. Ibrahim, M. Chshiev, A. Quintana, A. Lopeandia, M. O. Liedke, M. Butterling, E. Hirschmann, A. Wagner, L. Abad, J. L. Costa-Krämer, E. Menéndez, and J. Sort, ACS Appl. Mater. Interfaces **13**(26), 30826–30834 (2021).
[133]J. de Rojas, A. Quintana, A. Lopeandía, J. Salguero, B. Muñiz, F. Ibrahim, M. Chshiev, A. Nicolenco, M. O. Liedke, M. Butterling, A. Wagner, V. Sireus, L. Abad, C. J. Jensen, K. Liu, J. Nogués, J. L. Costa-Krämer, E. Menéndez, and J. Sort, Nat. Commun. **11**, 5871 (2020).
[134]S. Vasala, A. Jakob, K. Wissel, A. I. Waidha, L. Alff, and O. Clemens, Adv. Electron. Mater. **6**, 1900974 (2020).
[135]M. Huang, M. U. Hasan, K. Klyukin, D. Zhang, D. Lyu, P. Gargiani, M. Valvidares, S. Sheffels, A. Churikova, F. Büttner, J. Zehner, L. Caretta, K.-Y. Lee, J. Chang, J.-P. Wang, K. Leistner, B. Yildiz, and G. S. D. Beach, Nat. Nanotechnol. **16**, 981 (2021).
[136]P. D. Murray, C. J. Jensen, A. Quintana, J. Zhang, X. Zhang, A. J. Grutter, B. J. Kirby, and K. Liu, ACS Appl. Mater. Interfaces **13**(32), 38916–38922 (2021).
[137]J. Zehner, R. Huhnstock, S. Oswald, U. Wolff, I. Soldatov, A. Ehresmann, K. Nielsch, D. Holzinger, and K. Leistner, Adv. Electron. Mater. **5**, 1900296 (2019).
[138]Z. Mustafa, D. Pravarthana, B. Wang, H. Yang, and R.-W. Li, Phys. Rev. Appl. **14**, 014062 (2020).
[139]C. Navarro-Senent, A. Quintana, E. Isarain-Chávez, E. Weschke, P. Yu, M. Coll, E. Pellicer, E. Menéndez, and J. Sort, ACS Appl. Mater. Interfaces **12**, 14484–14494 (2020).
[140]C. Navarro-Senent, J. Fornell, E. Isarain-Chávez, A. Quintana, E. Menéndez, M. Foerster, L. Aballe, E. Weschke, J. Nogués, E. Pellicer, and J. Sort, ACS Appl. Mater. Interfaces **10**, 44897 (2018).
[141]S. Robbennolt, P. Yu, A. Nicolenco, P. Mercier Fernandez, M. Coll, and J. Sort, Nanoscale **12**, 5987 (2020).
[142]S. Robbennolt, E. Menéndez, A. Quintana, A. Gómez, S. Auffret, V. Baltz, E. Pellicer, and J. Sort, Sci. Rep. **9**, 10804 (2019).
[143]D. A. Gilbert, J. Olamit, R. K. Dumas, B. J. Kirby, A. J. Grutter, B. B. Maranville, E. Arenholz, J. A. Borchers, and K. Liu, Nat. Commun. **7**, 11050 (2016).
[144]K. Duschek, M. Uhlemann, H. Schlörb, K. Nielsch, and K. Leistner, Electrochem. Commun. **72**, 153 (2016).
[145]A. J. Grutter, D. A. Gilbert, U. S. Alaan, E. Arenholz, B. B. Maranville, J. A. Borchers, Y. Suzuki, K. Liu, and B. J. Kirby, Appl. Phys. Lett. **108**, 082405 (2016).
[146]K. Duschek, A. Petr, J. Zehner, K. Nielsch, and K. Leistner, J. Mater. Chem. C **6**, 8411 (2018).
[147]J. Zehner, O. Vaerst, I. Soldatov, K. Nielsch, R. Schafer, and K. Leistner, IEEE Trans. Magn. **58**, 6000108 (2021).
[148]T. Tsuchiya, K. Terabe, M. Ochi, T. Higuchi, M. Osada, Y. Yamashita, S. Ueda, and M. Aono, ACS Nano **10**, 1655 (2016).
[149]S. Robbennolt, A. Nicolenco, P. Mercier Fernandez, S. Auffret, V. Baltz, E. Pellicer, E. Menéndez, and J. Sort, ACS Appl. Mater. Interfaces **11**, 37338 (2019).
[150]A. Quintana, E. Menéndez, M. O. Liedke, M. Butterling, A. Wagner, V. Sireus, P. Torruella, S. Estradé, F. Peiró, J. Dendooven, C. Detavernier, P. D. Murray, D. A. Gilbert, K. Liu, E. Pellicer, J. Nogues, and J. Sort, ACS Nano **12**(10), 10291–10300 (2018).
[151]M. Cialone, A. Nicolenco, S. Robbennolt, E. Menéndez, G. Rius, and J. Sort, Adv. Mater. Interfaces **8**, 2001143 (2021).
[152]J. de Rojas, A. Quintana, A. Lopeandía, J. Salguero, J. L. Costa-Krämer, L. Abad, M. O. Liedke, M. Butterling, A. Wagner, L. Henderick, J. Dendooven, C. Detavernier, J. Sort, and E. Menéndez, Adv. Funct. Mater. **30**, 2003704 (2020).
[153]J. M. D. Coey and P. A. I. Smith, J. Magn. Magn. Mater. **200**, 405 (1999).
[154]H. A. Wriedt, N. A. Gokcen, and R. H. Nafziger, Bull. Alloy Phase Diagrams **8**, 355 (1987).
[155]J. Häglund, A. Fernández Guillermet, G. Grimvall, and M. Körling, Phys. Rev. B **48**, 11685 (1993).
[156]Z. T. Y. Liu, X. Zhou, S. V. Khare, and D. Gall, J. Phys.: Condens. Matter **26**, 025404 (2014).
[157]D. B. Strukov and R. S. Williams, Appl. Phys. A **94**, 515 (2009).
[158]Z. Tan, J. de Rojas, S. Martins, A. Lopeandia, L. Abad, A. Quintana, J. Salguero, M. Cialone, J. Herrero-Martín, J. Meersschaut, A. Vantomme,

© Author(s) 2022

J. L. Costa-Krämer, J. Sort, and E. Menéndez, "Brain-inspired magneto-ionics: emulation of stimulated and post-stimulated neural learning," (unpublished).
[159]M. Nastasi, J. Mayer, and J. K. Hirvonen, *Ion-Solid Interactions* (Cambridge University Press, New York, 1996).
[160]I. Kaur, Y. Mishin, and W. Gust, *Fundamentals of Grain and Interphase Boundary Diffusion*, 3rd ed. (John Wiley & Sons, Inc., New York, 1995).
[161]M. Lerch, J. Janek, K. D. Becker, S. Berendts, H. Boysen, T. Bredow, R. Dronskowski, S. G. Ebbinghaus, M. Kilo, M. W. Lumey, M. Martin, C. Reimann, E. Schweda, I. Valov, and H. D. Wiemhöfer, Prog. Solid State Chem. **37**, 81 (2009).
[162]C. J. Jensen, A. Quintana, M. Sall, L. H. Diez, J. Zhang, X. Zhang, D. Ravelosona, and K. Liu, J. Magn. Magn. Mater. **540**, 168479 (2021).
[163]Y. Gu, C. Song, Q. Wang, W. Hu, W. Liu, F. Pan, and Z. Zhang, APL Mater. **9**, 040904 (2021).
[164]R. Sarmiento-Pérez, T. F. T. Cerqueira, S. Körbel, S. Botti, and M. A. L. Marques, Chem. Mater. **27**, 5957 (2015).

© Author(s) 2022